NMR Investigation of Main-Chain Dynamics of the H80E Mutant of Bovine Neurophysin-I: Demonstration of Dimerization-Induced Changes at the Hormone-Binding Site†

Mandar T. Naik, Hunjoong Lee, Clay Bracken,* and Esther Breslow*

Department of Biochemistry, Weill Medical College of Cornell University, 1300 York Avenue, New York, New York 10021

Received March 3, 2005; Revised Manuscript Received July 8, 2005

ABSTRACT: Neurophysins are hormone-binding proteins composed of two partially homologous domains. Ligand-binding (localized to the amino domain) and dimerization (involves both domains) are cooperatively linked by an as yet undefined allosteric mechanism. To help define this mechanism, we investigated the backbone dynamics of the unliganded monomeric state of the H80E mutant of bovine neurophysin-I by ^{15}N NMR. Model-free analysis of the NMR relaxation parameters indicated significantly greater flexibility in the carboxyl domain than in the amino domain**,** particularly at their dimerization interface segments. Amino domain residues critical to hormone binding were highly structured, constraining potential allosteric mechanisms. Model-free analysis additionally demonstrated chemical exchange effects, manifest as R_{ex} terms, in 16 residues, 14 of which are located in the amino domain at, or immediately adjacent to, either the dimerization interface or the hormone-binding site. The chemical exchange process was further characterized using relaxation-compensated CPMG measurements, the results allowing assignment of the process to monomer−dimer exchange and calculation of the exchange kinetics, which were slow on the NMR time scale. An apparently different concentration-dependent process, distinguished from normal dimerization by its fast exchange behavior and pH-independence, also principally involved a subset of residues at and immediately adjacent to either the hormone-binding site or the amino domain dimerization interface. The data represent the first direct demonstration of an effect of dimerization in the unliganded state on neurophysin's hormone-binding site, the effect particularly involving residues that interact with hormone residue 2, and specifically identify Ser25 and Ile26 as likely intermediaries between the sites of dimerization and of hormone binding. Consistent with recent views of the role of anchor residues in protein interactions, we propose that dimerization proceeds by a fast pH-independent association of the well-structured amino domain interface that is rapidly communicated to the binding site for hormone residue 2**,** followed by a rate-determining pH-dependent interaction of the less structured carboxyl domain interface.

Ligand-facilitated protein self-association is an essential contributor to many biological pathways, and mechanisms underlying the phenomenon have been of significant interest (e.g., *1*−*4*). In the case of neurophysin (NP),[1] ligand-facilitated self-association plays an important role in the targeting of the common precursors of neurophysins and the hormones oxytocin and vasopressin to neurosecretory granules, the neurophysin dimerization constant increasing by a factor of approximately 100 upon binding of hormone or analogous smaller peptides (e.g., *5*−*9***)**. This represents the thermodynamic equivalent of a 10-fold stronger binding of peptide by a dimer subunit than by an isolated monomer (*9*) and is an allosteric effect, since the sites of binding and dimerization are not proximal (e.g., *10*). Moreover, because subunit interface changes associated with binding to the dimer are small (*10*) and because the rate of binding to dimer subunits is significantly greater than the rate of binding to monomer (*11* and unpublished studies by this laboratory), conformational differences between unliganded monomers and dimers are likely to play an important role (*10*). The nature of these conformational differences is unknown. Although the conformation of the unliganded dimeric state of des 1-6 bovine NP-II (des 1-6 BNP-II) has been solved

† Supported by NIH Grant GM-17528.

* To whom correspondence should be addressed. Mailing address: Department of Biochemistry, Weill Medical College of Cornell University, 1300 York Avenue, New York, NY 10021. Fax: 212-746-8875. C.B.: phone, 212-746-6473; e-mail, wcb2001@med.cornell.edu. E.B.: phone, 212-746-6428; e-mail, ebreslow@med.cornell.edu.

[1] Abbreviations: NP, neurophysin; BNP-I, bovine neurophysin I (oxytocin-related bovine neurophysin); H80E, the H80E mutant of BNP-I; BNP-II, bovine neurophysin II (vasopressin-related bovine neurophysin II); des 1-6 BNP-II, BNP-II from which the first six residues have been excised; WT, wild type; HPLC, high-pressure liquid chromatography; MALDI-TOF, matrix assisted laser desorption ionization time-of-flight; 1D, one-dimensional; HSQC, heteronuclear single quantum coherence; R_1, spin−lattice relaxation rate constant; R_2, transverse relaxation rate constant; R_{ex}, apparent chemical exchange contribution to R_2; NOE, nuclear Overhauser effect; rc-CPMG experiment, relaxation compensated Carr−Purcell−Meiboom−Gill experiment; τ_{cp}, interpulse delay time in rc-CPMG experiment; τ_m, overall correlation time; τ_e, internal correlation time; k_{ex}, microscopic chemical exchange rate; S^2, generalized order parameter; DSS, 2,2-dimethyl-2-silapentane-5-sulfonic acid.

10.1021/bi0504153 CCC: $30.25
Published on Web 08/12/2005

crystallographically (*10*), and the conformation of the unliganded monomeric state of the weakly dimerizing H80E mutant of bovine NP-I (BNP-I) has been solved by NMR (*12*),[2] these proteins share only ~75% identity, so that the residual sequence differences between the two prevent unambiguous interpretation of the significance of their structural differences.

Allosteric phenomena can involve changes in average protein conformation and/or protein dynamics, both mechanisms amenable to NMR analysis. The availability of the H80E mutant of BNP-I, which retains the allosteric properties of its parent protein despite its low dimerization constant in the unliganded state (*13*), allows NMR investigation of the dynamics of chain motion in the monomer and the effects of monomer−dimer exchange on individual residues *within the same protein*. Here we report the results of ^{15}N spin relaxation studies, which provide the first demonstration of an effect of dimerization on the hormone-binding site and new insights into allosteric mechanism. For reference we note that BNP-I is a 93 amino acid protein with seven disulfide bridges (e.g., *5*). It is divided by disulfide-pairing and homology relationships into an amino-domain (residues 1−54) and a carboxyl domain (residues 59−93), the carboxyl domain having strong homology to residues 11−44 of the amino domain (*14*, *15*); the unstructured region 55−58 is essentially an interdomain loop. Figure 1 diagrams the 2° structure a neurophysin chain as seen in both NP crystal and NMR structures. It also indicates the residues involved in dimerization and in the critical (e.g., *5*) binding interactions with the hormone α-amino group and tyrosine ring in position 2. Essentially all of the residues significantly involved in hormone binding are located in the amino domain, while dimerization principally involves the antiparallel self-association of corresponding segments from both domains.

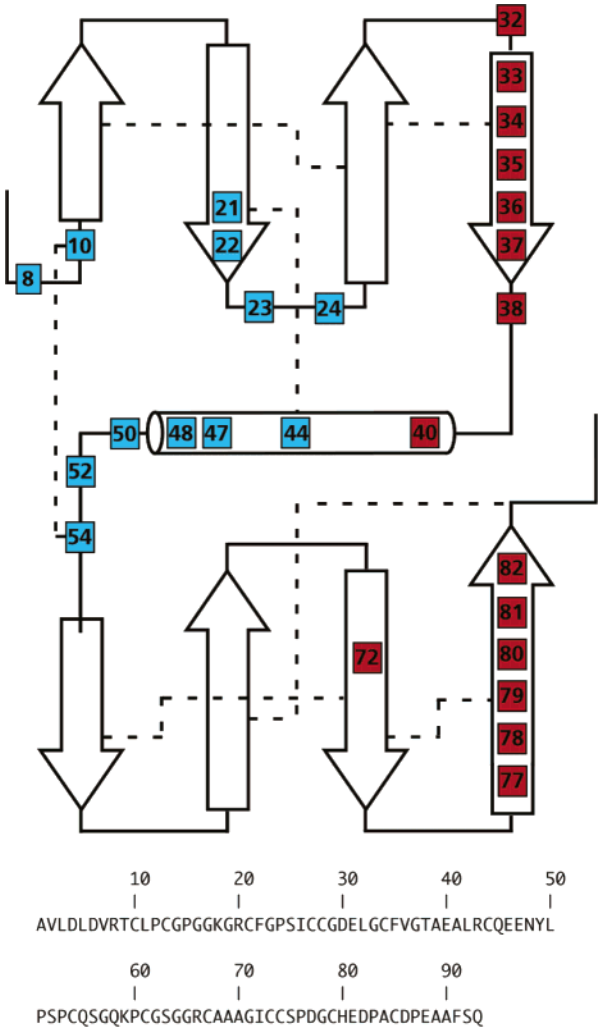

FIGURE 1: Secondary structure of bovine NPII dimer subunits as deduced from BNPII crystal structures (e.g., *10*, *15*); dashed lines show disulfide connectivities. The secondary structure of H80E in the unliganded monomeric state is similar (*12*). Beta sheet residues are 11−15, 17−22, 25−29, 33−37, 59−61, 65−68, 71−75, and 77−82. The 3,10 helix is composed of residues 39−48. Numbered residues in red are those at the subunit interface of the dimer, as defined by interactions at ≤4 Å with the partner subunit. Numbered residues in blue are those that interact at ≤4 Å with either the α-amino group, the tyrosine ring, or the hydroxyl group of the peptide ligand. The amino acid sequence of wild-type BNPI (*39*) is shown below for reference.

MATERIALS AND METHODS

Protein Preparation and Purification. The H80E mutant of BNP-I was overexpressed as a fusion protein along with a His tag and TrpLe leader peptide in *Escherichia coli* BL21 (DE3) strain under control of the T7 promoter, as previously described (*13*). Note that our recombinant BNP-I and mutants thereof lack residue 93, for which no significant role is known (*16* and references therein). Uniform ^{15}N isotope labeling was achieved by Marley's media exchange protocol (*17*) optimized for H80E expression (*12*). The isolation of fusion protein and subsequent CNBr cleavage, purification, and folding, followed by final affinity separation from misfolded protein, were performed as described earlier (*13*, *16*). The purity of ^{15}N-labeled H80E was ascertained by gel electrophoresis, HPLC, and MALDI-TOF spectroscopy.

NMR Relaxation Data Acquisition and Processing. H80E samples for NMR were prepared by dissolving uniformly ^{15}N labeled protein in 250 μL of 1:9 D_2O/H_2O. The pH was adjusted to 7.5 (uncorrected for deuterium effects) by small additions of dilute HCl or NaOH. No buffer was used in the NMR sample; the intrinsic buffer capacity of the concentrated protein was sufficient to maintain the pH, which was checked following NMR experiments. All NMR experiments were performed in Shigemi NMR tubes (Shigemi Inc., Allison Park, PA). The temperature was calibrated using ethylene glycol and maintained at 30 °C. Data were acquired on a Varian Inova 600 MHz spectrometer equipped with a 5 mm triple resonance gradient probe. The chemical shifts for ^{1}H and ^{15}N were indirectly referenced (*18*) to the ^{2}H lock resonance of water at 30 °C, giving a value of ^1H_2O of 4.70 ppm relative to external 2,2-dimethyl-2-silapentane-5-sulfonic acid (DSS).

The ^{15}N spin−lattice relaxation rate constant (R_1), transverse relaxation rate constant (R_2), and steady-state heteronuclear {^{1}H}-^{15}N nuclear Overhauser effects (NOEs) were

[2] The different approaches used to date to analyze BNP-I and -II reflect the fact that BNP-II and its derivatives have historically proven easier to crystallize than BNP-I, but less suitable for NMR, because of decreased solubility at high concentrations. However, both wild type proteins dimerize too strongly to permit analysis of their monomeric states by either technique, so the weakly dimerizing H80E mutant of BNP-I was engineered (*13*) to permit analysis of the all-monomer state at NMR-accessible concentrations.

measured using gradient enhanced heteronuclear correlation experiments (*19*, *20*). Ten R_1 experiments were performed in random order, with relaxation delays of 10 (in duplicate), 30, 60, 120, 220 (in duplicate), 330, 550, and 990 ms. Similarly R_2 experiments were performed with relaxation delays of 10 (in duplicate), 30, 50, 70, 110 (in duplicate), 150, 190, and 230 ms collected in randomized order. The NOE experiments were carried out with and without proton saturation and repeated three times. All experiments were acquired with 1280 × 96 complex points in ^{1}H and ^{15}N dimensions with corresponding spectral widths of 10 000 and 1700 Hz. The data sets were processed using nmrPipe (*21*) and analyzed using Sparky (*22*). Peak intensities were integrated and the data fitted to an exponential decay using the Sparky software. Errors in the relaxation rates were estimated by Monte Carlo simulations with statistics taken from 500 or more rounds of curve fittings. Each NOE was calculated as the ratio of peak intensity collected with proton saturation to that collected without proton saturation. The error figures in the NOE measurements were obtained by error propagation from the base plane signal-to-noise.

Chemical Exchange. The chemical exchange processes that contribute to transverse relaxation rates were directly measured using relaxation compensated Carr−Purcell−Meiboom−Gill (rc-CPMG) experiments. The $R_2(1/\tau_{cp})$ rates were collected with interpulse delay values, τ_{cp}, of 1, 2, 5 × 2, 10, and 15 ms at 1 mM total protein concentration, pH 7.5, 30 °C (*23*). The contribution of monomer−dimer chemical exchange was further characterized at 2 mM sample concentration. Values of $\Delta R_2(1/\tau_{cp})$ were measured using τ_{cp} values of 1 ms and 10 ms. The relaxation rate, $R_2(1/\tau_{cp})$, for all time scales is given by (*24*−*26*)

$$R_2(1/\tau_{cp}) = (1/2)(R_M + R_D + k_{ex} - 1/\tau_{cp}\cdot\cosh^{-1}[D_+ \cosh(\eta_+) - D_- \cosh(\eta_-)]) \quad (1)$$

$$D_\pm = \frac{1}{2}\left[\pm 1 + \frac{\psi + 2\Delta\omega^2}{\sqrt{\psi^2 + \zeta^2}}\right]$$

$$\eta_\pm = \frac{\tau_{cp}}{\sqrt{2}}[\sqrt{\pm\psi + (\psi^2 + \zeta^2)^{1/2}}]$$

$$\psi = (R_M + R_D - p_M k_{ex} + p_D k_{ex})^2 - \Delta\omega^2 + 4p_M p_D k_{ex}^2$$

$$\zeta = 2\Delta\omega(R_M - R_D - p_M k_{ex} + p_D k_{ex})$$

where R_M and R_D are the transverse relaxation rates for monomer and dimer populations, p_M and p_D (= 1 − p_M) are their respective weight fractions, and $\Delta\omega$ is the chemical shift difference in radians/s between these two exchanging sites. In the present work, the relaxation, $R_2(1/\tau_{cp})$, was evaluated for short τ_{cp} delays of 1, 2, and 5 ms by the original pulse sequence and long delays of 5, 10, and 15 ms by a modified sequence (*23*, *26*). The duplicate 5 ms data point ensured reproducibility between data sets collected by the two sequences.

Diffusion Anisotropy. Estimates of the diffusion anisotropy for unliganded NP monomer and dimer conformations were calculated using the monomer solution structure of the H80E mutant of BNP-I (PDB codes 1L5C and 1L5D) and the dimer crystal structure of des 1-6 BNP-II (PDB code 1JK6). The crystallographic structures were protonated using the MOLMOL molecular graphics package for analysis of molecular diffusion. Measurement of the inertial diffusion tensor was made using the "pdbinertia" program (Prof. A. G. Palmer, Columbia University), and estimates of the hydrodynamic radii were assessed using HYDRONMR (*27*). Solution anisotropy was estimated from relaxation rates using the QUADRIC DIFFUSION program (A. G. Palmer, Columbia University) as described by Tjandra et al. **(***28***).** The relaxation rates employed for estimates of anisotropy and correlation times were selected using the protocols of Tjandra et al. and excluding residues undergoing chemical exchange identified using the 600 MHz R_2R_1 product cutoff value as defined by Kneller et al. (*29*).

Model-Free Analysis. The amide ^{15}N nuclear spins in proteins relax by two main mechanisms, viz., dipolar coupling with their attached proton and anisotropy of ^{15}N chemical shifts. The movement of the NH bond axis, as characterized by the spectral density function, describes the internal and overall motions of the molecule. Equations for R_1, R_2, and the steady-state NOE can be written in terms of the model-free spectral density functions that describe these molecular motions **(***30*, *31***)**. The model-free analysis considers five semiempirical forms of the spectral density function, sequentially attempting to fit the data to the simplest of five increasingly complex models. The simplest of these generates an order parameter term, S^2, while the more complex models generate both S^2 and terms relating to the correlation times of internal motions (τ_e) that are shorter than the overall correlation time and/or to chemical exchange (R_{ex}), as described in detail by Mandel et al. (*32*). The amide bond length was fixed to 1.02 Å, and ^{15}N chemical shift anisotropy was estimated as −170 ppm in our calculations. All these motional parameters were fitted to the spin relaxation data by using the program Model-Free 4.01 (*32*, *33*).

For each model, 800 randomly distributed data sets were generated and discrimination between models was performed using *F*-statistic analysis (*32*). These steps were automatically performed with Model-free using Fast Model-free (*34*).

Chemical Shift Assignments. Backbone amide chemical shift assignments used are those of Nguyen and Breslow (*12*), with the exception, based on a reassessment of HNCOCA, HNCA, and ^{15}N NOESY HSQC (heteronuclear single quantum coherence) connectivities, of the reassignment of the signal originally assigned to the −NH of Gly57 to a second signal from Gly23. The reassignment adds Gly57 to the earlier list (*12*) of residues (Cys10, Glu31, Gly62, Gly64, and Asp86) with unassigned signals and adds Gly23 to the list, comprising approximately a quarter of the residues (*12*), exhibiting signal heterogeneity (more than one HSQC signal).[3] Dynamics data were obtained on all assigned signals that were sufficiently strong and well resolved. Data for

[3] The reassignment additionally explains the originally ambiguous NOE between this signal and an unidentified signal (*12*) as one between Phe22 and Gly23 and essentially restricts the derived conformation to that (*12*) representing the absence of an NOE to Gly57. It is also relevant to stress that the H80E signal heterogeneity does not represent the presence of impurities. The heterogeneity is independent of the preparation, as we have previously noted (*12*), with more recent studies indicating that it is also present in the WT protein and reduced in prevalence at low pH. Potential sources of the signal heterogeneity include isomerization of one or more of the 9 proline residues and 7 disulfide bridges.

Table 1: Average Order Parameters for Selected Protein Regions[a]

structural element (sequence)	residues solved	average S^2
amino domain	37	0.867 (±0.039)
carboxyl domain	23	0.744 (±0.028)
β1 (11−15)	2	0.940 (± 0.086)
β2 (17−22)	6	0.921 (± 0.066)
β3 (25−29)	5	0.913 (± 0.052)
β4 (33−37)	4	0.938 (±0.046)
{amino domain dimer interface}		
H1 (39−48)	6	0.980 (±0.024)
β5 (59−61)	2	0.756 (±0.177)
β6 (65−68)	4	0.881 (±0.061)
β7 (71−75)	4	0.917 (±0.027)
β8 (77−82)	5	0.732 (±0.084)
{carboxyl domain dimer interface}		
critical peptide binding residues (8, 10, 21−24, 44, 47, 48, 50, 52, 54)[b]	10	0.949 (±0.052)

[a] Minor signals of residues exhibiting signal heterogeneity are not included. [b] Critical binding site residues are defined as those with contacts of ≤4 Å to either the peptide α-amino group or the Tyr-2 ring and −OH group. Of these, residue 10 is unassigned and residue 24 is Pro.

Table 2: Chemical Exchange Parameters for 1 mM H80E at pH 7.5 and 303 K from rc-CPMG Analysis[a]

residue	structure	R_2^0 (s^{-1})	$\Delta\omega$ (s^{-1})	k_{ex} (s^{-1})	p_M
Leu11	β1	13.8 (±1.4)	210 (±45)	76 (±31)	0.72
Gly14	β1	13.1 (±0.6)	638 (±2051)	90 (±52)	0.98
Gly14[b]	β1	11.2 (±0.8)	452 (±246)	153 (±67)	0.97
Cys21	β2	12.9 (±0.4)	260 (±190)	90 (±75)	0.99
Cys21[b]	β2	12.7 (±1.0)	462 (±323)	95 (±65)	0.95
Phe22[c]	β2	13.5 (±0.4)	289 (±257)	214 (±290)	0.99
Ile26[b]	β3	10.3 (±1.2)	223 (±193)	93 (±55)	0.87
Cys27	β3	12.3 (±0.3)	340 (±485)	140 (±31)	0.99
Cys28	β3	11.4 (±0.9)	770 (±250)	90 (±13)	0.97
Gly29	β3	11.3 (±0.8)	1078 (±286)	117 (±39)	0.98
Gly33	β4	10.4 (±0.2)	1196 (±68)	91 (±15)	0.96
Cys34	β4	11.6 (±1.2)	1065 (±484)	102 (±26)	0.96
Leu42	H1	16.0 (±0.8)	1052 (±205)	263 (±39)	0.98
Lys59[c]	β5	11.6 (±0.4)	252 (±60)	132 (±373)	0.99
Arg66	β6	9.6 (±0.2)	204 (±43)	90 (±24)	0.97
Cys67	β6	10.7 (±0.0)	477 (±83)	115 (±34)	0.98
Ala68	β6	10.4 (±0.3)	1094 (±334)	70 (±23)	0.98
Ala69		9.0 (±0.1)	1065 (±143)	105 (±6)	0.98
Ala69[b]		12.5 (±0.8)	874 (±322)	118 (±39)	0.94
Cys73	β7	11.5 (±0.3)	194 (±13)	85 (±10)	0.97
Ser75	β7	10.5 (±0.1)	218 (±35)	97 (±18)	0.95
Asp77	β8	14.0 (±0.8)	188 (±217)	70 (±36)	0.95
Gly78	β8	8.1 (±0.2)	242 (±53)	115 (±43)	0.97

[a] R_2^0 (s^{-1}) is the value of R_2 calculated in the absence of exchange. $\Delta\omega$ (s^{-1}) is the calculated difference in chemical shift between monomer and dimer signals, expressed as radians/s. p_M is the calculated weight fraction of monomer. [b] Minor component of heterogeneous signal as described in ref *12*. [c] Values for this signal not included in calculations because of large uncertainty in k_{ex}.

residues 5, 56, 72, and 91 were deleted from consideration because of overlap between the signals of 5 and 72 and of 56 and 91. For the majority of residues exhibiting signal heterogeneity, the derived order parameters of their different signals were in reasonable agreement, although occasional differences of undetermined significance were found (Results, Tables 2 and 3, and Supporting Information).

RESULTS

Determination of Dimerization Constants. Direct measurement of NP dimerization constants by one-dimensional (1D) NMR involves determination, as a function of protein concentration, of the relative intensities of the Cys28 α-proton signal in the monomeric and dimeric states (e.g., *35*); in the H80E mutant, these are located at ∼6.2 and 6.4 ppm, respectively, and are in slow chemical exchange with respect to high field NMR time scales (*13*). The dimerization constant of the H80E mutant was previously shown to be pH-dependent (*12, 13*) and was estimated to be less than 100 M^{-1} at pH 7.5, but to increase on lowering the pH. We re-evaluated the dimerization constant of H80E at pH 7.5 by acquiring the 1D proton spectra using an increased number of acquisitions and different protein concentrations. The dimerization constant at pH 7.5 and 30 °C was estimated as 62 ± 32, leading to monomer weight fractions of 0.90 and 0.83 at 1 mM and 2 mM protein concentration. As will be seen below, the dimerization constant can also be calculated by rc-CPMG experiments, these experiments giving an average value at pH 7.5 and 30 °C of 32 ± 4 M^{-1}, representing monomer weight fractions of 0.95 and 0.89 at 1 mM and 2 mM concentrations, respectively, and corresponding to the lower range of the values obtained in the 1D studies. It has been shown that dynamics parameters decrease in reliability as conformational purity decreases below 90% (*36*). Accordingly, we used 1 mM H80E at pH 7.5 for most of our relaxation experiments as the best compromise between signal-to-noise ratio and reliable measurements.

Several HSQC spectra were obtained at pH 6.6 (vide infra). The dimerization constant at this pH under HSQC solvent conditions had been calculated earlier as 330 ± 10 M^{-1} between 298 K and 308 K (*12*, *13*, and unpublished data) and is used in interpretation of the pH 6.6 data.

Effect of Protein Concentration on HSQC Spectra. HSQC spectra collected as a function of concentration indicated the presence of both fast and slow kinetic processes. A slow time scale for the interconversion beween monomer and dimer was originally suggested (but see also Discussion) by temperature-jump and stopped-flow methodology for BNP-I at pH 3.8 (*37*). This was subsequently demonstrated by NMR

Table 3: Chemical Exchange Parameters for 2 mM H80E at pH 7.5 and 303 K from rc-CPMG Analysis[a]

residue	structure	R_2^0 (s^{-1})	$\Delta\omega$ (s^{-1})	k_{ex} (s^{-1})	p_M
Cys13	β1	12.9 (±0.7)	210 (±16)	127 (±87)	0.92
Gly14	β1	12.6 (±0.9)	661 (±304)	93 (±40)	0.98
Phe22	β2	16.8 (±0.5)	164 (±85)	63 (±57)	0.89
Cys28[b]	β3	12.1 (±1.6)	181 (±98)	490 (±831)	0.85
Cys28[c]	β3	12.5 (±1.8)	194 (±55)	411 (±377)	0.84
Gly29[b]	β3	14.1 (±1.6)	531 (±189)	71 (±87)	0.86
Leu42[c]	H1	13.7 (±0.7)	1318 (±964)	98 (±42)	0.96
Cys44	H1	16.7 (±0.8)	395 (±391)	103 (±37)	0.83
Cys44[c]	H1	14.0 (±1.2)	510 (±325)	97 (±62)	0.89
Ala68[b]	β6	12.8 (±1.4)	342 (±77)	317 (±327)	0.96
Ala69		12.5 (±1.1)	194 (±17)	271 (±234)	0.92
Ala70		21.0 (±0.5)	202 (±45)	67 (±26)	0.67
Cys74[b]	β7	14.7 (±0.4)	163 (±22)	63 (±96)	0.62
Cys74[c]	β7	12.6 (±1.2)	408 (±119)	87 (±38)	0.91
Ser75	β7	12.6 (±0.6)	525 (±158)	133 (±86)	0.95
Gly78[b]	β8	9.9 (±1.0)	172 (±29)	373 (±1293)	0.93
Glu80	β8	11.5 (±0.6)	1681 (±274)	192 (±54)	0.97

[a] R_2^0 (s^{-1}) is the value of R_2 calculated in the absence of exchange. $\Delta\omega$ (s^{-1}) is the calculated difference in chemical shift between monomer and dimer signals, expressed as radians/s. p_M is the calculated weight fraction of monomer. [b] Values for this signal not included in calculations because of large uncertainty in k_{ex}. [c] Minor component of heterogeneous signal as described in ref *12*.

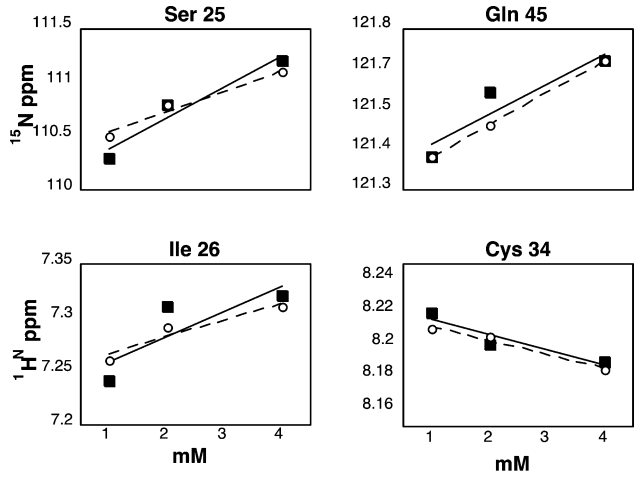

FIGURE 2: Effects of protein concentration on the chemical shifts of the peptide bond HSQC signals of Ser25 (N), Ile 26 (H), Cys34 (H), and Gln45 (N). For residues exhibiting signal heterogeneity, data shown are for the principal signal. Black squares and solid line, pH 7.5; open circles and dashed line, pH 6.6. (Lines are to guide the eye only.)

at both neutral and low pH for BNP-I and -II, as well as for the H80E and other mutants of BNP-I, monitoring the behavior of the Cys28 α-proton as described above (e.g., *13*, *35*). We collected HSQC spectra at pH 7.5 and 6.6 at 1 mM, 2 mM, and 4 mM protein chain concentration and observed that a subset of cross peaks (representing residues Gly23, Ser25, Ile26, Cys34, Glu40, and Gln45, and including both principal and secondary signals in cases of signal heterogeneity) are clearly concentration-dependent at both pH values, with behavior suggesting fast exchange between two environments on the NMR time scale, and with no evidence of a significant pH dependence in this pH interval despite the different dimerization constants involved. Representative examples are shown in Figure 2. All the fast exchange atoms are in the amino domain (Figure 1), and no carboxyl domain residues exhibiting this behavior were identified. Additional cross peaks corresponding to dimer appear in new regions of the HSQC spectrum as the concentration is increased, representing residues for which exchange is slow on the NMR time scale.

Relaxation Rates and NOE Data. The relaxation parameters for 70 residues out of a total of 92 (of which 9 are Pro) were reliably quantitated. Values of R_1, R_2, and NOE's, obtained at 1 mM concentration, pH 7.5, are shown in Figure 3. As found for most other native proteins, the longitudinal relaxation rates, R_1, are constant throughout the sequence except for decreases in both terminal regions. On the other hand, transverse relaxation rates, R_2, show significant variation in magnitude across the sequence. The high value of R_2 for Ser25 is particularly striking, such large values being generally attributed to chemical exchange or motional anisotropy. The NOE data also appear to be similar to data obtained with other native proteins with the two less restricted terminal regions (regions outside the central disulfide paired region consisting of residues 10−85) falling to negative values. Lower than average NOE values are also exhibited by Gln58 of the interdomain loop and Lys59. The 10% trimmed average values of the relaxation parameters are $R_1 = 2.033 \pm 0.072$ s^{-1}, $R_2 = 8.356 \pm 0.308$ s^{-1}, and NOE $= 0.604 \pm 0.038$.

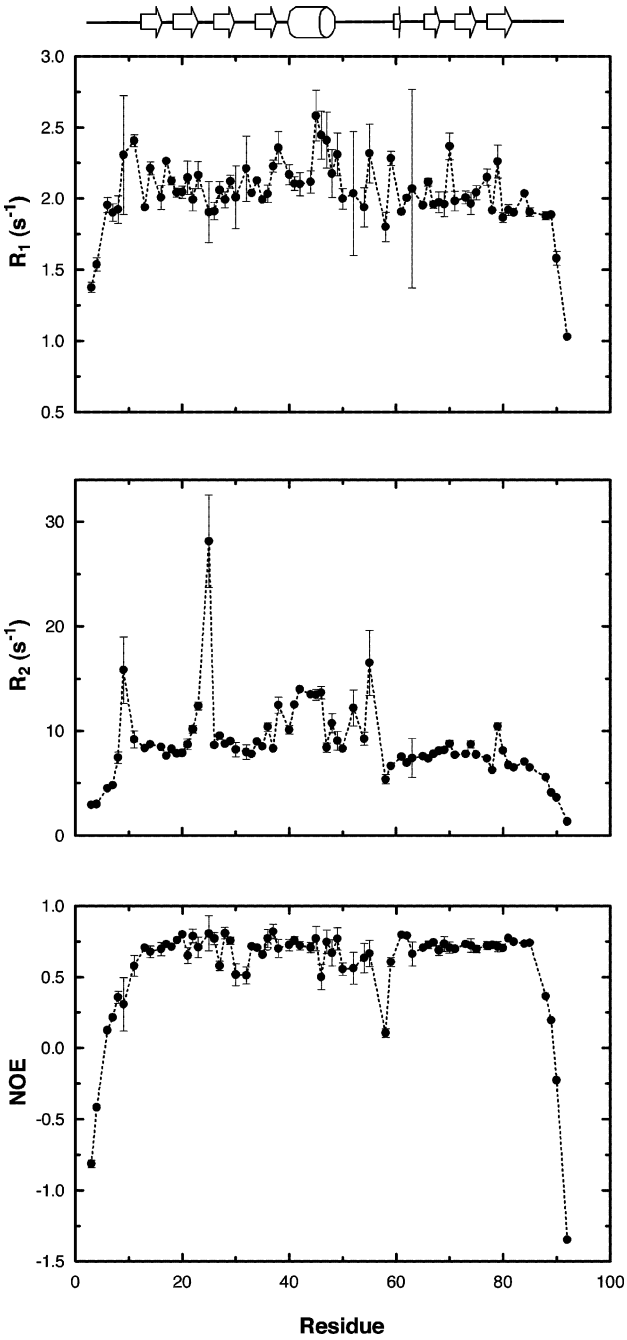

FIGURE 3: Backbone amide spin relaxation parameters for H80E at 14.1 T. The values of R_1, R_2, and heteronuclear NOE are plotted as a function of residue number in primary sequence. The diagram on top is a schematic representation of H80E secondary structure. Conditions: 1 mM protein at pH = 7.5 and 303 K. Data for secondary components of the heterogeneous signals are not shown for simplicity.

Calculations of backbone dynamics from the relaxation data rest in part on assumptions about molecular shape. Both monomers and dimers are oblate in conformation in the neurophysin NMR and crystallographic structures. Analysis of these static structural models indicated an anisotropy tensor of 1.00:0.89:0.52 in the H80E monomer and a ratio of 1.00:0.92:0.50 in the des 1-6 BNP-II dimer crystal structure. However, based on the observed relaxation data, no clear relationship between relaxation rate and orientation relative to molecular axes was observed and no statistical improvement in the model-free fits was observed upon

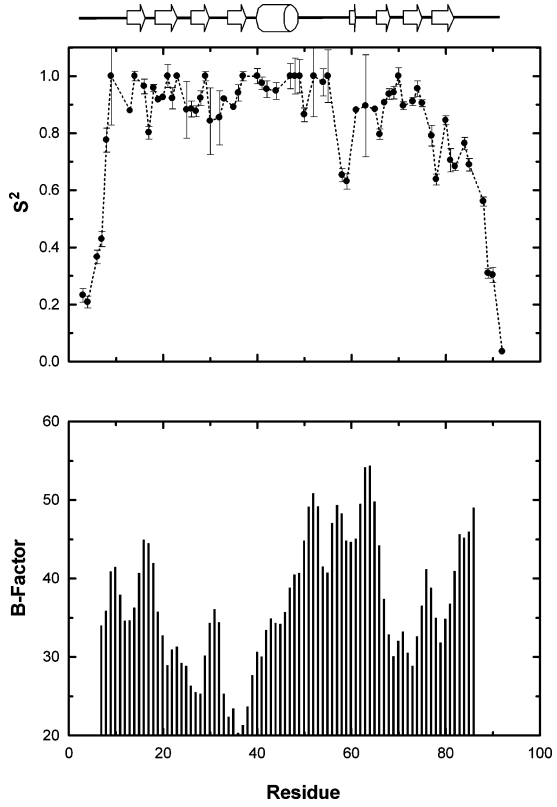

FIGURE 4: Comparison of H80E order parameters, S^2, calculated from the extended model-free analysis, with average *B*-factors for the two chains of the unliganded des 1-6 BNP-II dimer crystal structure (*10*; PDB code: 1JK6).

inclusion of molecular diffusion anisotropy tensors. Furthermore, calculation of the overall correlation time (τ_m) using the R_2/R_1 ratios resulted in $\tau_m = 5.19$ ns, which closely agrees with isotropic estimates of the rotational correlation time, $\tau_m = 5.43$ ns, based on the isotropic Stokes−Einstein equation. By contrast, estimation of the effective correlation time based on the static molecular structure using the HYDRONMR program (*27*) suggested an average correlation time of 6.27 ns. These results indicated that an isotropic model was more suitable for analysis of the relaxation data.

Model-Free Analysis. Of the 70 residues analyzed, the data for 63 could be satisfactorily fitted to one of the several program models. The relaxation behavior of Leu11, Cys34, Thr38 (main signal only), Gln45, Glu46, Ile72, and Cys79 could not be adequately described by any of the models. The generalized order parameters (S^2) determined from model-free fitting are plotted as a function of amino acid sequence in Figure 4 and are listed for selected regions of the protein in Table 1. In Figure 5, they are also encoded on the solution structure of H80E, with $(1 - S^2)$ proportional to the ribbon width. A table summarizing the results of the model-free analysis for individual residues is provided in the Supporting Information. Of particular interest is the significantly higher order of the amino domain than of the carboxyl domain (Table 1). This difference is only in part accounted for by the high degree of order in the 3,10 helix that is unique to the amino domain. Despite the strong conformational homology between the β-sheet regions of the amino and carboxyl domains (e.g., *15*), the average order of amino domain β-sheet residues is significantly higher than that of carboxyl domain β-sheet residues; differences between the segments

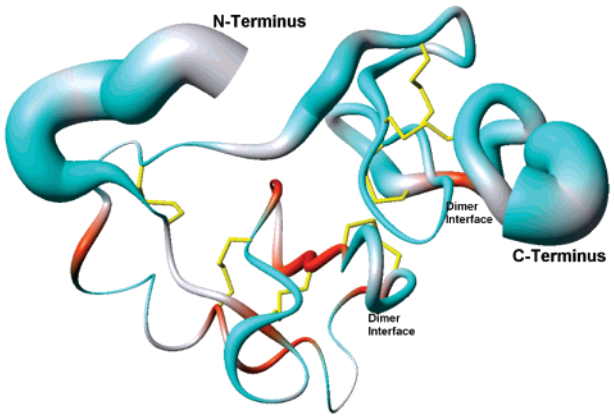

FIGURE 5: Sausage representation of the H80E NMR solution structure (PDB code 1L5D) with the ribbon width proportional to $1 - S^2$. The sausage is shown in red for residues showing ms−μs motions as identified by the R_{ex} term in model-free calculations. Proline and other residues for which relaxation parameters could not be quantitated are shown in gray with the sausage radius interpolated from neighboring residues. Disulfide bonds are shown in yellow. The figure was constructed with program MolMol (*43*).

representing the amino domain and carboxyl domain dimer interfaces are particularly striking (Table 1). Also of interest is that analyzable residues involved in the most critical binding interactions with hormone, as defined in Figure 1 (residues 8, 21−23, 44, 47, 48, 50, 52, 54), display particularly high order parameters (Table 1).

Figure 4 also compares the derived order parameter plot with a plot of the *B* factors derived from the crystal structure of unliganded dimeric des 1-6 BNP-II (*10*). The two plots differ in the relative degree of flexibility suggested for the helix and succeeding loop region (vide infra). However, the difference between the carboxyl and amino domains in β-sheet order is also manifest in dimer *B*-factors, where it again indicates greater mobility of the interface segment of the carboxyl domain than of the amino domain (cf., residues 32−40 vs 77−82).

Model-free analysis also indicated the presence of picosecond motions that are on a shorter time scale (τ_e) than the overall rotational correlation time (τ_m). Values of τ_e are plotted in Figure 6 and tend to show an inverse correlation with order parameters. Thus, the highest concentration of residues with motions on the picosecond/nanosecond time scale are at the chain termini and the detected motions are more concentrated in distribution in the more poorly ordered carboxyl domain than in the amino domain, the differences again particularly striking when the interface regions of the two domains are compared.

Conformational exchange between different environments that occurs on the same time scale as the change in chemical shift can give rise to line broadening of the NMR resonance, increasing apparent R_2 values. The model-free approach accommodates such exchange and other pseudo-first-order processes by introducing the term R_{ex}. The majority of the residues with significant R_{ex} contributions reside in the amino domain as shown in Figure 6 and its caption; all of these are direct participants in binding or dimerization, or are in direct contact at <4 Å with residues involved in these processes. For example, residues 22, 23, 44, and 50 bind directly to hormone, while residues 35, 36, and 38 bind to the partner subunit. It is also noteworthy (see Discussion)

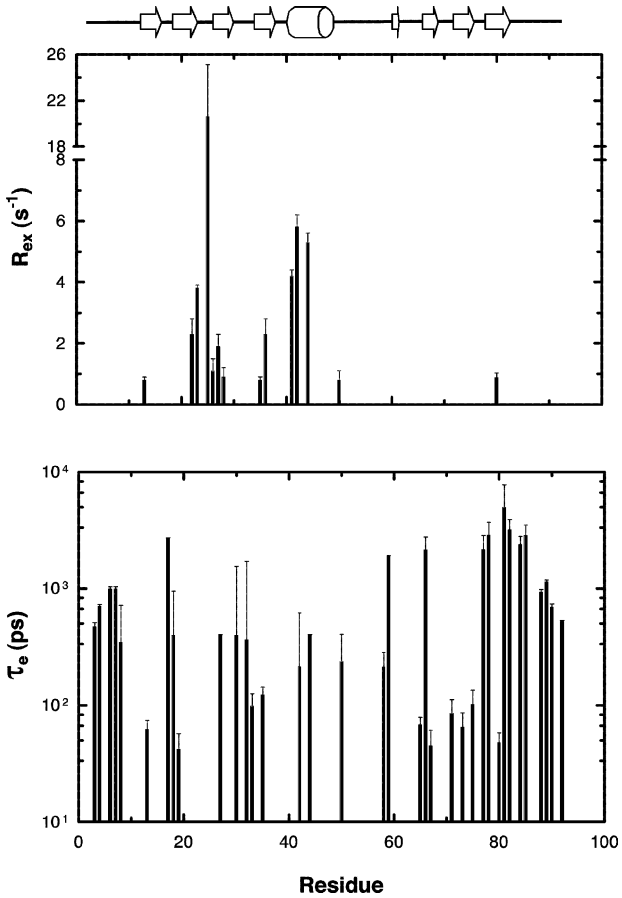

FIGURE 6: Backbone dynamics of 1 mM H80E BNP-I. Chemical exchange contribution, R_{ex}, and internal correlation time, τ_e, are plotted against residue number. For residues exhibiting signal heterogeneity, only the properties of their principal signals are shown in the plots. However, chemical exchange contributions to the relaxation properties of the secondary signals of residues 38 (5.6/s) and 69 (5.1/s) are present.

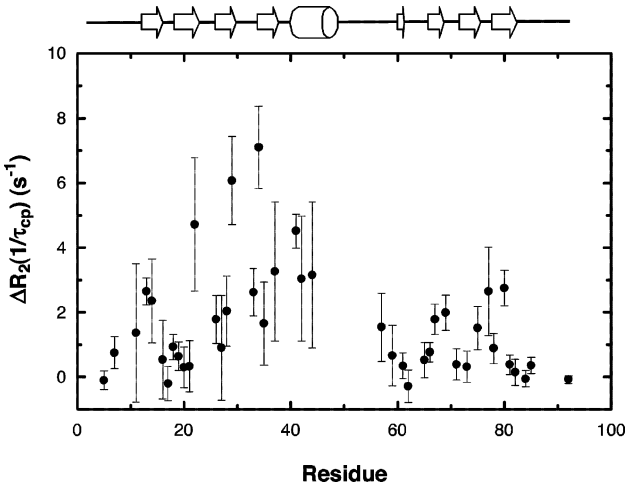

FIGURE 7: Evidence of chemical exchange in H80E at pH 7.5 and 303 K by rc-CPMG experiment. The plotted value $\Delta R_2(1/\tau_{cp})$ was determined as the measured relaxation rate at $\tau_{cp} = 10$ ms minus that at $\tau_{cp} = 1$ ms. Positive values of $\Delta R_2(1/\tau_{cp})$ indicate regions of microsecond to millisecond conformational exchange.

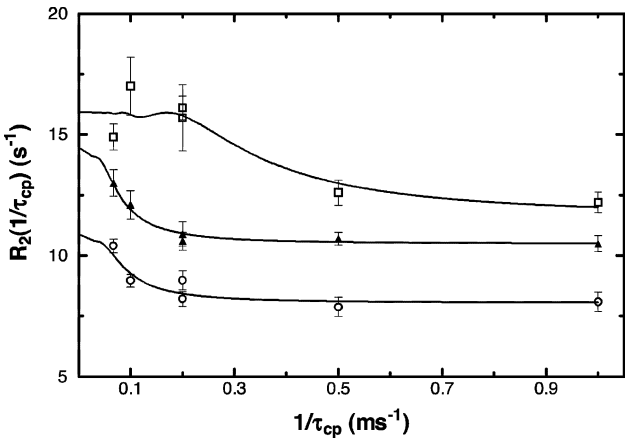

FIGURE 8: rc-CPMG dispersion curves for selected residues in H80E BNP-I. $R_2(1/\tau_{cp})$ is plotted as a function of $1/\tau_{cp}$ and fitted to the full CPMG equation. Data were obtained in a separate experiment from those in Figure 7 and are shown for three residues: square, C34; filled triangle, S75; circle, G78. Lines show the fit of the data to the equation.

that residues 22, 23, and 44, which exhibit much larger values of R_{ex} than residue 50, interact with the Tyr-2 ring of the hormone, while residue 50 interacts with the hormone α-amino group. Of the two carboxyl domain residues showing significant R_{ex} values, residue 80 is directly at the carboxyl domain dimerization interface (e.g., *10*). Thus, of residues exhibiting significant values of R_{ex}, only carboxyl domain residue 69 is neither at nor immediately adjacent to either the binding site or the interface. The fact that four dimerization interface residues (residues 35, 36, 38, and 80) exhibit significant R_{ex} values suggests the contribution of monomer−dimer interconversion to R_{ex}.

Relaxation Compensated CPMG Measurement. The rc-CPMG experiment (*23*, *26*, *38*) was used to confirm the presence of exchange and to quantitate the microscopic chemical exchange rates (k_{ex}) for residues involved in exchange processes. Qualitative observation of chemical exchange at multiple backbone sites was evident from positive differences in $\Delta R_2(1/\tau_{cp})$ as measured at long ($\tau_{cp} = 10$ ms) and short ($\tau_{cp} = 1$ ms) interpulse delays (Figure 7). A good dispersion $R_2(1/\tau_{cp})$ against $1/\tau_{cp}$, as shown in Figure 8 for a few representative residues of H80E, is crucial for meaningful calculations. Values of k_{ex} for appropriately behaved residues, calculated at 1 and 2 mM protein concentrations, are given in Tables 2 and 3. Note that several residues exhibiting significant values of R_{ex}, including residues Ser25 and Gly23, could not be evaluated by this method, largely reflecting low signal intensities. The results independently confirm the existence of conformational exchange throughout the amino domain of H80E, as initially suggested by the model-free analysis, and also support the more limited effect of these exchange processes on the carboxyl domain, as evidenced by the significantly lower values of $\Delta R_2(1/\tau_{cp})$ for carboxyl domain residues than for those in the amino domain in Figure 7. Nonetheless, several more carboxyl domain residues are implicated in these exchange processes by the rc-CPMG experiments than by the model-free R_{ex} calculations as seen in Tables 2 and 3. Excluding values for which the uncertainty was greater than the mean (see table footnotes) and trimming to remove values for which the variance from the mean was ≥3× the average variance, calculated values of k_{ex} were 100 ± 23 (SD) s^{-1} and 106 ± 37 (SD) s^{-1} at 1 mM and 2 mM concentrations, respectively. It is noteworthy that the occasional outliers are randomly distributed and are not consistent at the two concentrations. Also, both binding site residues (e.g., residues 21, 22, 44) and interface residues (e.g., residues 33, 34, 77,

78, 80) show no consistent difference in their calculated kinetics, and no significant difference is seen between amino domain and carboxyl domain residues. Thus the rc-CPMG results likely reflect a single exchange process that affects multiple residues throughout the protein. It is relevant also that the derived value of k_{ex} is considerably greater than the value of <10/s estimated (*12*) to be responsible for signal heterogenity, confirming that the processes involved are nonidentical.

An added bonus of the rc-CPMG data is that, assuming that the exchange process monitored is monomer−dimer exchange (see Discussion), the results include estimates of p_M, the weight fraction of monomer in each sample (Tables 2 and 3), which in turn allowed an independent estimate of the dimerization constant. Average monomer weight fractions of 0.95 at 1 mM concentration and 0.89 at 2 mM concentration yielded a dimerization constant of 32 ± 4 M^{-1} as reported above.

DISCUSSION

Comparative Dynamics of the Two Domains. The present results demonstrate clear differences in the dynamics of the two domains of the H80E monomer that contrast with the marked conformational homology of their β-sheet regions demonstrated by crystallography (e.g., *15*). Both the order parameters and the distribution of residues with picosecond/nanosecond motions indicate a greater flexibility of carboxyl domain β-sheet regions than of those of the amino domain, the difference extending to the two dimerization interface regions. As indicated above, a lesser degree of order in the β-sheet regions of the carboxyl domain than in the amino domain is also evident from the distribution of crystallographic *B*-factors in the unliganded des 1-6 dimer of bovine NP-II (Figure 4). Because the H80E mutant of bovine NP-I particularly differs from des 1-6 BNPII in carboxyl domain sequence (*39*), the shared carboxyl domain flexibility of the two appears to be a common feature of neurophysins in both monomeric and dimeric unliganded states. This additionally suggests that the introduction of the position 80 mutation in H80E is not the fundamental cause of the disorder in its carboxyl domain. While it cannot be precluded that the mutation exacerbates the disorder, it is relevant that the order parameter of E80 is significantly higher than that of its immediate neighbors (Supporting Information).

Nature of the Chemical Exchange Process Expressed by k_{ex}. We assign the exchange process responsible for the rc-CPMG data to monomer−dimer interchange. This assignment is supported by the fact that a number of the residues yielding k_{ex} values are interface residues (residues 33, 34 77, 78, 80), while the signals of several others (residues 26, 28, 68) are otherwise known (e.g., *12*) to be altered by dimerization. The respectable agreement between the dimerization constant derived from the rc-CPMG studies based on this assumption and that derived from 1D NMR studies (vide supra) further supports this assignment. The data therefore allow some insights into the kinetics of monomer−dimer interchange. Thus (*40*), for a monomer−dimer exchange system,

$$k_{ex} = 2(M)k_{on} + k_{off} \quad (2)$$

where (M) is the equilibrium concentration of monomer, k_{on} is the dimerization rate constant, and k_{off} is the dimer dissociation rate constant. Assuming a dimerization constant at pH 7.5 of 62 M^{-1} as determined from 1D studies (see above), $k_{off} = k_{on}/62$. Using the above equation, calculation of the rate constants from the average values of k_{ex} at 1 mM and 2 mM total chain concentration (vide supra) gives average values for k_{on} and k_{off} at pH 7.5 and 30 °C of 5.7×10^3 M^{-1} s^{-1} and 9.1×10^1 s^{-1}, respectively.

A single earlier study represented an investigation of the dimerization kinetics of WT bovine NPI at pH 3.8 using dye-binding as a probe (*37*). The derived kinetic parameters ($k_{on} \sim 10^5$ M^{-1} s^{-1}, $k_{off} \sim 10$ s^{-1}) compare reasonably with those here given the difference in pH and the fact that the WT protein dimerizes more strongly than H80E, but the earlier results are in part compromised by the fact that the dye-binding model to which the data were fitted was potentially inapplicable (*41*). However, regardless of other data, it is relevant that the association rate constant we calculate is several orders of magnitude lower than a diffusion-limited bimolecular rate constant. Since the dimerization constant of the mutant (as well as of the WT protein) increases as the pH decreases (e.g., *13*), the low apparent association rate constant must in part reflect the participation in the rate-determining step only of the subset of residues that are appropriately protonated, which is not considered in the above calculation, and/or the necessity for conformational change during or prior to this step as further discussed below.

Nature of Fast Exchange Concentration-Dependent Changes in HSQC Spectra. While we attribute the exchange processes responsible for the CPMG data to formation and dissociation of the normal dimer, other intermolecular processes appear also to be operative, as evidenced by the fast exchange concentration-dependent changes in chemical shift for the peptide bond HSQC signals of residues 23, 25, 26, 34, 40, and 45. The fact that chemical shifts for these residues are essentially the same at each concentration at pH 6.6 and 7.5 (Figure 2) strongly argues against assignment of these effects to the normal pH-dependent monomer−dimer equilibrium. The dimerization constant of H80E in 90% water/10% D_2O (HSQC conditions) estimated by 1D NMR studies at pH 6.6 is ~5× that estimated at pH 7.5 by the same methodology (vide supra). On the basis of the 1D NMR dimerization constants, the fractional content of dimer at 1 mM, pH 6.6, is essentially the same as that at 4 mM, pH 7.5, and the dimer content at 4 mM concentration, pH 6.6, is twice that at 4 mM, pH 7.5. Assuming fast exchange, if the changes in HSQC chemical shift with concentration represented the normal monomer−dimer equilibrium, chemical shifts for these residues at pH 6.6 should be significantly shifted toward pH 7.5 values characteristic of higher concentration, which is not the case. Moreover, again assuming fast exchange between monomer and dimer, if we calculate a hypothetical difference beween monomer and dimer chemical shifts at either pH from the change in chemical shift with increasing dimer concentration, the results indicate that the exchange rate of 100/s between monomer and dimer is too low to generate fast exchange behavior on the NMR time scale.

So what type of process is represented by the fast exchange transition? Nonspecific aggregation seems unlikely given the relative linearity of the concentration dependence over the range studied. Alternatively, we note that all residues involved in the fast exchange transition appear so far to be

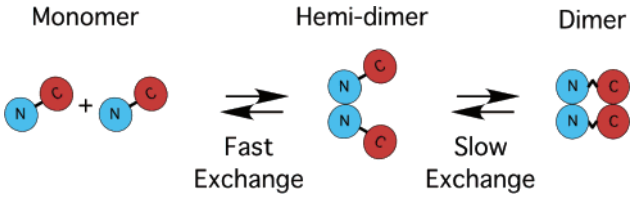

FIGURE 9: Proposed dimerization kinetic scheme for H80E. Conformational change within the amino domain is proposed to accompany both steps of the reaction to account for all the data. Conformational change within the carboxyl domain is most likely to accompany the second step.

in the amino domain, that residues 34 and 40 are interface residues, and that residues 23, 25, and 26 have previously been suggested to participate in the communication between the binding site and subunit interface responsible for the subtle interface changes that accompany peptide-binding to the dimer (*6*). Gly23 is a ligand for the aromatic ring in position 2 of bound peptides, interaction with the ring tightening its interactions with Ile26 and Ser25, two residues that in turn contact interface residues from the same subunit (e.g., see Figure 1). Gln45 is in close contact (<3.5 Å) with Pro24, which is probably the principal protein contact of the peptide aromatic ring in position 2. Thus one possible explanation of the fast exchange results might be a weak transient interaction of this region with an aromatic ring on another chain. However, such interactions have only been observed for aromatic rings at position 2 of ligand peptides (e.g., *5*), a situation not represented in the protein.

Alternatively, we propose that the fast exchange reaction represents a weak, reversible self-association reaction of two chains solely via their amino domain interface regions, communicated to the binding site for peptide residue 2 by subtle conformational change, but not yet locked in by the rate-determining slower self-association of the more weakly structured carboxyl domain interface. The lack of pH dependence is explained by the fact that the pH dependence of the dimerization constants of both WT BNP-I and the H80E mutant almost certainly reflects titratable groups at the carboxyl domain interface. The amino domain interface region of these proteins is identical to that of BNP-II, the dimerization of which lacks the pH dependence of WT and mutant BNP-I (cf., *6*, *13*), while the carboxyl domain interface regions of BNP-II and BNP-I significantly differ in titratable residue position and identity (e.g., *39*). Dimerization-induced conformational change involving the hormone-binding site is indicated, since the binding site residues affected by dimerization are not sufficiently close to the subunit interface to be affected simply by the proximity of the partner chain.

An overall dimerization mechanism, proposed on the basis of our hypothesis for the fast exchange reaction, is shown in Figure 9 and is characterized by a rapid preequilibration of monomer with the partial amino domain dimer, the latter reacting to form the complete dimer. Note that the equilibrium constant for formation of the partial dimer, through which the reaction is proposed to proceed, is expected to be significantly lower than that for the overall dimerization reaction. Therefore, since the dynamics studies are carried out at low equilibrium concentrations of the complete dimer, the equilibrium concentration of the partial dimer, which determines the rate of formation of the complete dimer, should be negligible relative to that of monomer, helping to explain the low calculated value of k_{on}. Also, the fact that values of k_{ex} are the same for both amino domain and carboxyl domain residues suggests dominance of the observable kinetics by the interchange between monomer and the complete dimer. This may reflect the fact that these are the principal species present or a situation in which the effect of carboxyl domain association on amino domain conformation dominates that arising from formation of the partial dimer. The lack of a demonstrable contribution of the fast exchange reaction to the observed kinetics is also indicated by the fact that comparison (*38*) of the derived k_{ex} values of individual residues in Tables 2 and 3 with the derived values of $\Delta\omega$ indicates that most of the exchange rates measured, including those of Ile26 and Cys34, which exhibit the fast exchange reaction, are in the slow NMR exchange rate regime.

We assume a low probability for the simultaneous self-association of both amino and carboxyl domains upon the same monomer−monomer collision. Given this and the fact that the backbone conformation of the amino domain dimerization interface appears to undergo little change upon dimerization (*12*), the proposed mechanism is consistent with the higher degree of order of the amino domain interface than of the carboxyl domain interface, the extra rigidity potentially allowing more efficient bonding during collision. In this context, it is relevant that the amino domain segment of the interface is almost invariant among mammalian neurophysins, while this is not true of the carboxyl domain interface region (e.g., *39*), suggesting the importance of an initial rigid contact between subunits that stabilizes the complex during rearrangement of supporting contacts.

Recent evidence suggests that the fast exchange process seen here is not observable in WT BNP-I **(**unpublished observations**)**. This provides additional evidence against the possibility (vide supra) that the process involves binding of an aromatic protein side chain to the active site, since the WT protein retains all the aromatic residues of its H80E mutant. It instead suggests that the carboxyl domain interface region of the WT protein self-associates more rapidly than that of the mutant, the mutant compromised by the additional negative charge on its interface. A more rapid carboxyl domain self-association in the WT protein would have the potential to lock in the slowly dissociating complete dimer before the "partial dimer" could dissociate. None of these arguments rigorously preclude the possibility that formation of the amino domain hemidimer represents an abortive association of amino domains that is not on the direct path to formation of the complete dimer. However, we note that the dimerization mechanism independently proposed here based on the NMR data is consistent with the more general role of conformationally preconstrained residues as anchors in protein interactions, as very recently supported by molecular dynamics simulations (*42*).

Conclusions: Implications for Allosteric Mechanism. The current results provide strong support for a role for conformational differences between unliganded monomeric and dimeric states in contributing to ligand-facilitated dimerization. In particular, they provide the first unambiguous evidence—evidence uncomplicated by comparison of proteins with different primary structure—of a change in hormone-binding site conformation and/or environment upon dimer-

ization, specifically the binding site for the ring of Tyr-2 of the hormones. Three residues, 21, 22, and 44, in close (<4 Å) contact with the Tyr-2 ring and/or its −OH group, are clearly identified as perturbed by dimerization by rc-CPMG experiments. Residues 22 and 44 are also demonstrated to be in conformational exchange by model-free R_{ex} calculations, supporting the view that the model-free R_{ex} calculations and rc-CPMG analysis are sensing the same phenomenon. Residue 23 was not analyzable by the rc-CPMG experiment because of its weak HSQC signal, but is shown to be concentration-dependent and is identified to be in conformational exchange by model-free calculations. Finally, the demonstration by model-free calculations that both Ser25 and Ile26 are in conformational exchange, together with the concentration dependence of their chemical shifts, supports a potential role of these residues (*10*) as intermediaries between the binding site and subunit interface. Note that the original suggestion of a role for these residues as such intermediaries (*10*) was invoked to explain small changes in the dimerization interface associated with ligand-binding to the preexistent dimer, a process thermodynamically distinct from the effects here of dimerization on ligand-binding. A common pathway for both processes indicates its central role in neurophysin interactions.

Constraints on the possible nature of dimerization-induced binding site changes are suggested by the demonstration that binding site residues are relatively well ordered in the monomer. This finding particularly argues against mechanisms involving reduced binding site flexibility upon dimerization, such that the entropy loss on binding to the dimer is less than on binding to the monomer. More likely here is that dimerization involves a rearrangement within a relatively rigid section of the molecule that pre-positions atoms for more favorable interaction with hormone, and/or an increase in flexibility that reduces the uphill energy necessary to reposition binding site residues for optimal interactions with ligand. Some support for the increased flexibility thesis is found in the greater flexibility of the helix and succeeding loop region suggested by the des 1-6 BNP-II dimer crystal structure than by H80E monomer dynamics (vide supra), although potential interactions of residues 1−6 with the loop (e.g., *12*) might also account for this flexibility difference. Ongoing structural studies of the unliganded dimeric states of BNP-I and its H80E mutant should clarify these issues.

ACKNOWLEDGMENT

We gratefully acknowledge Professor Dinshaw Patel (Memorial Sloan Kettering Cancer Center) for providing NMR spectrometer time for several studies. We thank Professor Lewis E. Kay (University of Toronto) for providing Varian pulse sequences for measurement of R_1, R_2, and NOE values and Professor J. Patrick Loria (Yale University) for the rc-CPMG experiment pulse sequence. We are additionally grateful to Professor Arthur G. Palmer (Columbia University), to Professor Loria, and to the developers of Sparky and nmrPipe for other software used in this study. C.B. and E.B. are members of the New York Structural Biology Center supported by NIH Grant GM-66354.

SUPPORTING INFORMATION AVAILABLE

Backbone dynamics parameters for 1 mM H80E mutant of bovine neurophysin-I at pH 7.5 and 303 K from extended model-free analysis. This material is available free of charge via the Internet at http://pubs.acs.org.

REFERENCES

1. Holbro, T., and Hynes, N. E. (2004) ErbB receptors: directing key signaling networks throughout life, *Annu. Rev. Pharmacol. Toxicol. 44*, 195−317.
2. Schlessinger, J. (2002) Ligand-induced, receptor-mediated dimerization and activation of EGF receptor, *Cell 110*, 669−72.
3. Ferguson, K. M. (2004) Active and inactive conformations of the epidermal growth factor receptor, *Biochem. Soc. Trans. 32*, 742-5.
4. Surinya, K. H., Molina, L., Soos, M. A., Brandt, J., Kristensen, C., and Siddle, K. (2002) Role of insulin receptor dimerization domains in ligand binding, cooperativity and modulation by anti-receptor antibodies, *J. Biol. Chem. 277*, 16718−25.
5. Breslow, E., and Burman, S. (1990) Molecular, thermodynamic, and biological aspects of recognition and function in neurophysin-hormone systems: a model system for the analysis of protein-peptide interactions, *Adv. Enzymol. 63*, 1−67.
6. Nicolas, P., Batelier, G., Rholam, M., and Cohen, P. (1980) Bovine neurophysin dimerization and neurohypophyseal hormone binding, *Biochemistry 19*, 3565−73.
7. Kanmera, T., and Chaiken, I. M. (1985) Molecular properties of the oxytocin/bovine neurophysin biosynthetic precursor: studies using a semi-synthetic precursor, *J. Biol. Chem. 4*, 8474−82.
8. deBree, F. M., and Burbach, J. P. (1998) Structure-function relationships of the vasopressin prohormone domains, *Cell. Mol. Neurobiol. 18*, 173−91.
9. Breslow, E., LaBorde, T., Bamezai, S., and Scarlata, S. (1991) Binding and fluorescence studies of the relationship between neurophysin-peptide interaction and neurophysin self-association: an allosteric system exhibiting minimal cooperativity, *Biochemistry 30*, 7990−8000.
10. Wu, C. K., Bing, H., Rose, J. P., Liu, Z.-J., Nguyen, T. L., Zheng, C., Breslow, E., and Wang, B.-C. (2001) Structures of an unliganded neurophysin and its vasopressin complex: implications for binding and allosteric mechanisms, *Protein Sci. 10*, 1869−80.
11. Pearlmutter, A. F., and McMains, C. (1977) Interaction of bovine neurophysin with oxytocin and vasopressin measured by temperature-jump relaxation, *Biochemistry 16*, 628−33.
12. Nguyen, T. L., and Breslow, E. (2002) NMR analysis of the monomeric form of a mutant unliganded bovine neurophysin: comparison with the crystal structure of a neurophysin dimer, *Biochemistry 41*, 5920−30.
13. Eubanks, S., Nguyen, T., Peyton, D., and Breslow, E. (2000) Modulation of dimerization, binding, stability, and folding by mutation of the neurophysin subunit interface, *Biochemistry 39*, 8085−94.
14. Burman, S., Wellner, D, Chait, B., Chaudhary, T., and Breslow, E. (1989) Complete assignment of neurophysin disulfides indicates pairing in two separate domains, *Proc. Natl. Acad. Sci. U.S.A. 86*, 29−433.
15. Chen, L., Rose, J. P., Breslow, E., Yang, D., Chang, W. R., Furey, W. F. Jr., Sax, M., and Wang, B.-C. (1991) Crystal structure of a bovine neurophysin II dipeptide complex at 2.8 Å determined from the single-wavelength anomalous scattering signal of an incorporated iodine atom, *Proc. Natl. Acad. Sci. U.S.A. 88*, 4240−4244.
16. Eubanks, S., Lu, M., Peyton, D., and Breslow, E. (1999) Expression, folding and thermodynamic properties of the bovine oxytocin-neurophysin precursor: relationships to the intermolecular oxytocin-neurophysin complex, *Biochemistry 38*, 1530−41.
17. Marley, J., Lu, M., and Bracken, C. (2001) A method for efficient isotopic labeling of recombinant proteins, *J. Biomol. NMR 20*, 71−5.
18. Bracken, C., Carr, P. A., Cavanagh, J., and Palmer, A. G. (1999) Temperature dependence of intramolecular dynamics of the basic leucine zipper of GCN4: implications for the entropy of association with DNA, *J. Mol. Biol. 285*, 2133−46.
19. Skelton, N. J., Palmer, A. G., Akke, M., Kordel, J., Rance, M., and Chazin, W. J. (1993) Practical Aspects of Two-dimensional proton-detected ^{15}N spin relaxation measurements, *J. Magn. Reson. 102*, 253−64.

20. Farrow, N. A., Muhandiram, R., Singer, A. U., Pascal, S. M., Kay, C. M., Gish, G., Shoelson, S. E., Pawson T., Forman-Kay, J. D., and Kay, L. E. (1994) Backbone dynamics of a free and phosphopepide-complexed Src homology 2 domain studied by 15N NMR relaxation, *Biochemistry 33*, 5984−6003.
21. Delaglio, F., Grzesiek, S., Vuister, G. W., Zhu, G., Pfeifer, J., and Bax, A. (1995) NMRPipe: a multidimensional spectral processing system based on UNIX pipes, *J. Biomol. NMR 6*, 277−93.
22. Goddard, T. D., and Kneller, D. G., *SPARKY 3*, University of California, San Francisco.
23. Loria, J. P., Rance, M., and Palmer, A. G. (1999) A Relaxation-compensated Carr-Purcell-Meiboom-Gill sequence for characterizing chemical exchange by NMR spectroscopy, *J. Am. Chem. Soc. 121*, 2331−2.
24. Millet, O. M., Loria, J. P., Kroenke, C. D., Pons, M., and Palmer, A. G. (2000) The static magnetic field dependence of chemical exchange line-broadening defines the NMR chemical shift time scale, *J. Am. Chem. Soc. 122*, 2867−77.
25. Carver, J. P., and Richards, R. E. (1972) A general two-site solution for the chemical exchange produced dependence of T2 upon the Carr-Purcell pulse separation, *J. Magn. Reson. 6*, 89−105.
26. Davis, D. G., Perlman, M. E., and London, R. E. (1994) Direct measurements of the dissociation-rate constant for inhibitor-enzyme complexes via the T_1 rho and T_2 (CPMG) methods, *J. Magn. Reson. 104*, 266−75.
27. Garcia de la Torre, J., Huertas, M. L., and Carrasco, B. (2000) HYDRONMR: prediction of NMR relaxation of globular proteins from atomic-level structures and hydrodynamic calculations, *J. Magn. Reson. 147*, 138−46.
28. Tjandra, N., Feller, S. E., Pastor, R. W., and Bax, A. (1995) Rotational diffusion anisotropy of human ubiquitin from ^{15}N NMR relaxation, *J. Am. Chem. Soc. 117*, 12562−6.
29. Kneller, J., and Bracken, C. (2002) An effective method for the discrimination of motional anisotropy and chemical exchange, *J. Am. Chem. Soc. 124*, 1852−3.
30. Lipari, G., and Szabo, A. (1982) Model-free approach to the interpretation of nuclear magnetic resonance relaxation in macromolecules. 1. Theory and range of validity, *J. Am. Chem. Soc. 104*, 4546−59.
31. Lipari, G., and Szabo, A. (1982) Model-free approach to the interpretation of nuclear magnetic resonance relaxation in macromolecules. 2. Analysis of experimental results, *J. Am. Chem. Soc. 104*, 4559−70.
32. Mandel, A. M., Akke, M., and Palmer, A. G. (1995) Backbone dynamics of Escherichia coli ribonuclease HI: correlations with structure and function in an active enzyme, *J. Mol. Biol. 246*, 144−63.
33. Mandel, A. M., Akke, M., and Palmer, A. G. (1996) Dynamics of ribonuclease H: temperature dependence of motions on multiple time scales, *Biochemistry 35*, 16009−23.
34. Cole, R., and Loria, J. P., (2003) FAST-Modelfree: a program for rapid automated analysis of solution NMR spin-relaxation data, *J. Biomol. NMR 26*, 203−13.
35. Zheng, C., Peyton, D., and Breslow, E. (1997) Modulation of dimerization by residues distant from the interface in bovine neurophysin-II, *J. Pept. Res. 50*, 199−209.
36. Schurr, J. M., Babcock, H. P., and Fujimoto, B. S. (1994) A test of the model-free formulas. Effects of anisotropic rotational diffusion and dimerization, *J. Magn. Reson. 105*, 211−24.
37. Pearlmutter, A. F. (1979) Bovine neurophysin-I dimerization studied by rapid kinetic techniques, *Biochemistry 18*, 1672−6.
38. Palmer, A. G., Kroenke, C. D., and Loria, J. P. (2001) Nuclear magnetic resonance methods for quantifying microsecond-to-millisecond motions in biological macromolecules, *Methods Enzymol. 339*, 204−38.
39. Chauvet, M. T., Hurpet, D., Chauvet, J., and Acher, R. (1983) Identification of human neurophysins: complete amino acid sequences of MSEL- and VLDV-neurophysins, *Proc. Natl. Acad. Sci. U.S.A.* 80, 2839−43.
40. Hill, R. B., Bracken, C., deGrado, W. F., and Palmer, A. G., III (2000) Molecular motions and protein folding: characterization of the backbone dynamics and folding equilibrium of α_2D using 13C NMR spin relaxation, *J. Am. Chem. Soc. 122*, 11610−9.
41. Carlson, J. D., and Breslow, E. (1981) Interaction of bromophenol blue and related dyes with bovine neurophysin-I: use as a probe of neurophysin chemistry, *Biochemistry 20*, 5062−72.
42. Rajamani, D., Thiel, S., Vajda, S., and Camacho, C. J. (2004) Anchor residues in protein-protein interactions, *Proc. Natl. Acad. Sci. U.S.A. 101*, 11287−92.
43. Koradi, R., Billeter, M., and Wuthrich, K. (1996) MOLMOL: a program for display and analysis of macromolecular structures, *J. Mol. Graphics 14*, 2041−54.

BI0504153